SUPPORTING INFORMATION: E46K-like α-synuclein mutants increase lipid interactions and disrupt membrane selectivity

Matteo Rovere[1], Alex E. Powers[1], Julia C. Pitino[1], Luis Fonseca-Ornelas[1], Dushyant S. Patel[1], Alessandro Achille[2], Ralf Langen[3], Jobin Varkey[3], Tim Bartels[1,4]*.

From the [1]Ann Romney Center for Neurologic Diseases, Brigham and Women's Hospital and Harvard Medical School, Boston MA, 02115, USA; the [2]Department of Computer Science, University of California, Los Angeles, Los Angeles CA, 90095, USA; the [3]Zilkha Neurogenetic Institute, University of Southern California, Los Angeles CA, 90033, USA; [4]the Dementia Research Institute, University College London, London, WC1E 6BT, UK

*To whom correspondence should be addressed: Dementia Research Institute, University College London, London, Gower Street, Cruciform Building Wing 2.4, WC1E 6BT, UK. Phone: +44-20-31086814; E-mail: t.bartels@ucl.ac.uk

Figures S1–S6 and Tables S1–S3.

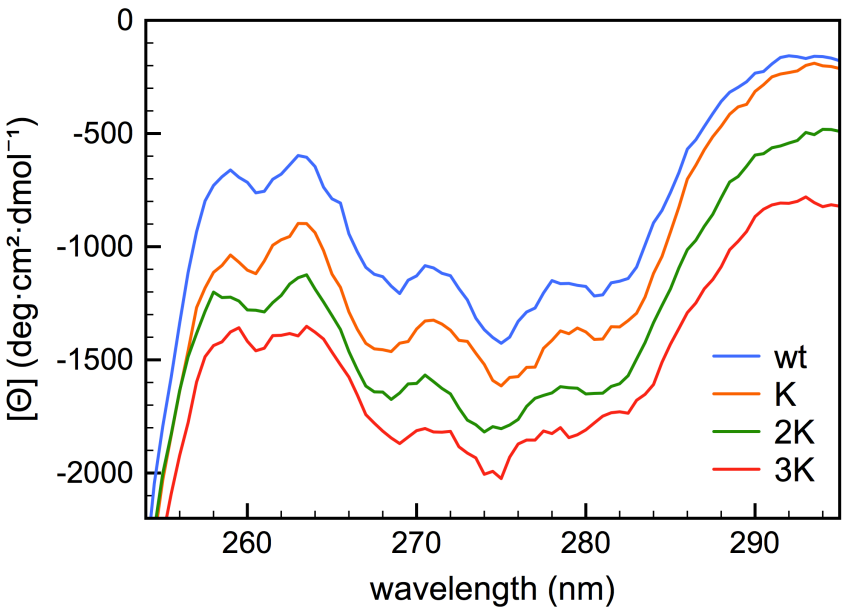

FIGURE S1. Near-UV CD spectra of 90 µM wt, K, 2K and 3K αSyn in 10 mM NH_4Ac, pH 7.40, measured at 25ºC. Spectra are arbitrarily offset for easier comparison. No clear differences among the E46K-like mutants are observed.

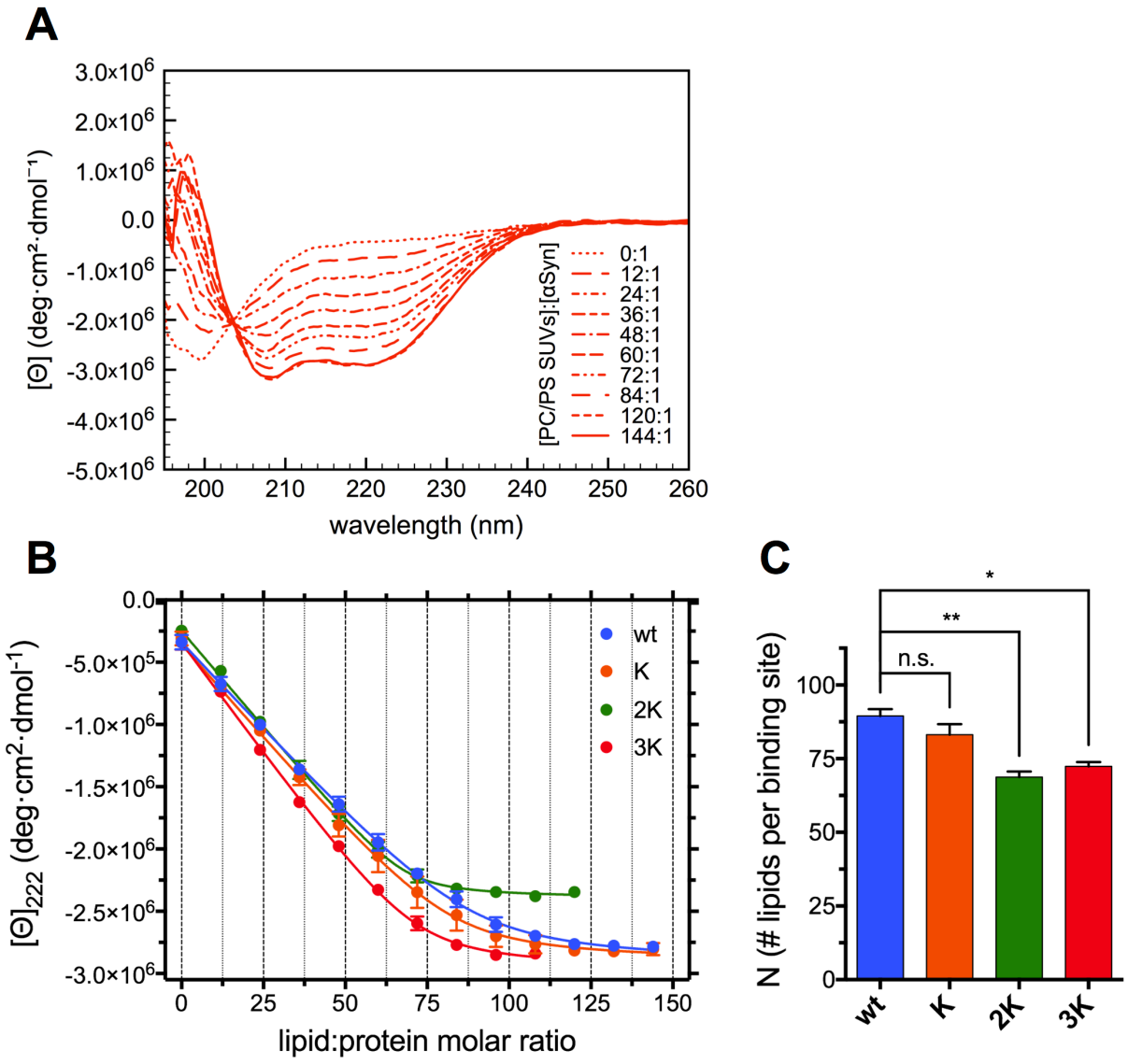

FIGURE S2. *A*, Representative far-UV CD spectra from a titration of 9.7 μM wt αSyn (in 9.7 mM NH_4Ac, 150 mM NaCl, pH 7.40) with 5.8 mM 70:30 POPC:DOPS SUVs, measured at 25ºC. *B*, Titration curves obtained from raw CD data after extracting the molar ellipticity at 222 nm and graphing it against the lipid:protein molar ratio at each point of the titration. Datapoints are shown along with their SEM (from *n*=3-6 independent titrations) and their best fit with an *N* independent binding sites model (*see* Experimental Procedures). *C*, Histogram of the *N* values (along with their SEM, *n*=3-6) obtained from the best fit of the titration curves with an *N* independent binding sites model. Decreasing *N*s indicate increased binding (or "avidity", *see* Results).

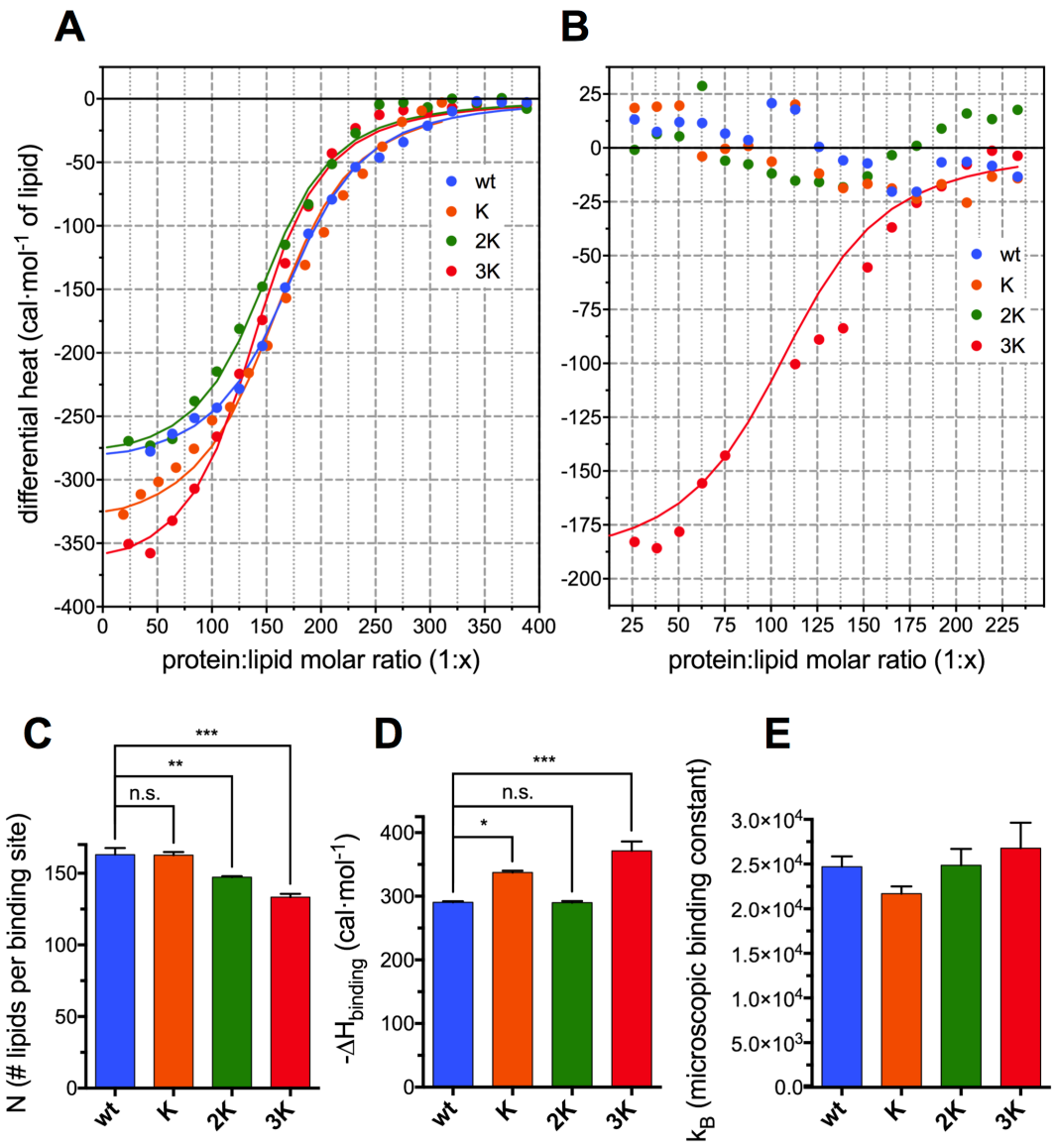

FIGURE S3. *A*, Representative ITC binding isotherms of 5 μM wt, K, 2K, and 3K αSyn (in 10 mM NH_4Ac, pH 7.40) with 6 mM 70:30 POPC:DOPS SUVs, measured at 25ºC. Datapoints are shown along with their best fit with an *N* independent binding sites model (*see* Experimental Procedures and Table S3). *B*, Representative ITC binding isotherms of 5 μM wt, K, 2K, and 3K αSyn (in 10 mM NH_4Ac, pH 7.40) with 6 mM 52.5:17.5:30 POPC:DOPS:cholesterol SUVs, measured at 25ºC. 3K αSyn datapoints are shown along with their best fit with an *N* independent binding sites model (*see* Experimental Procedures and Table S3). *C*, Histogram of the *N* values (along with their SEM, *n*=3) obtained from the best fit of the titration curves with an *N* independent binding sites model. Decreasing *N*s indicate increased binding (or "avidity", *see* Results). *D*, Histogram of the ΔH ($-\Delta H$) values (along with their SEM, *n*=3) obtained from the best fit of the titration curves with an *N* independent binding sites model. *E*, Histogram of the k_B values (along with their SEM, *n*=3) obtained from the best fit of the titration curves with an *N* independent binding sites model.

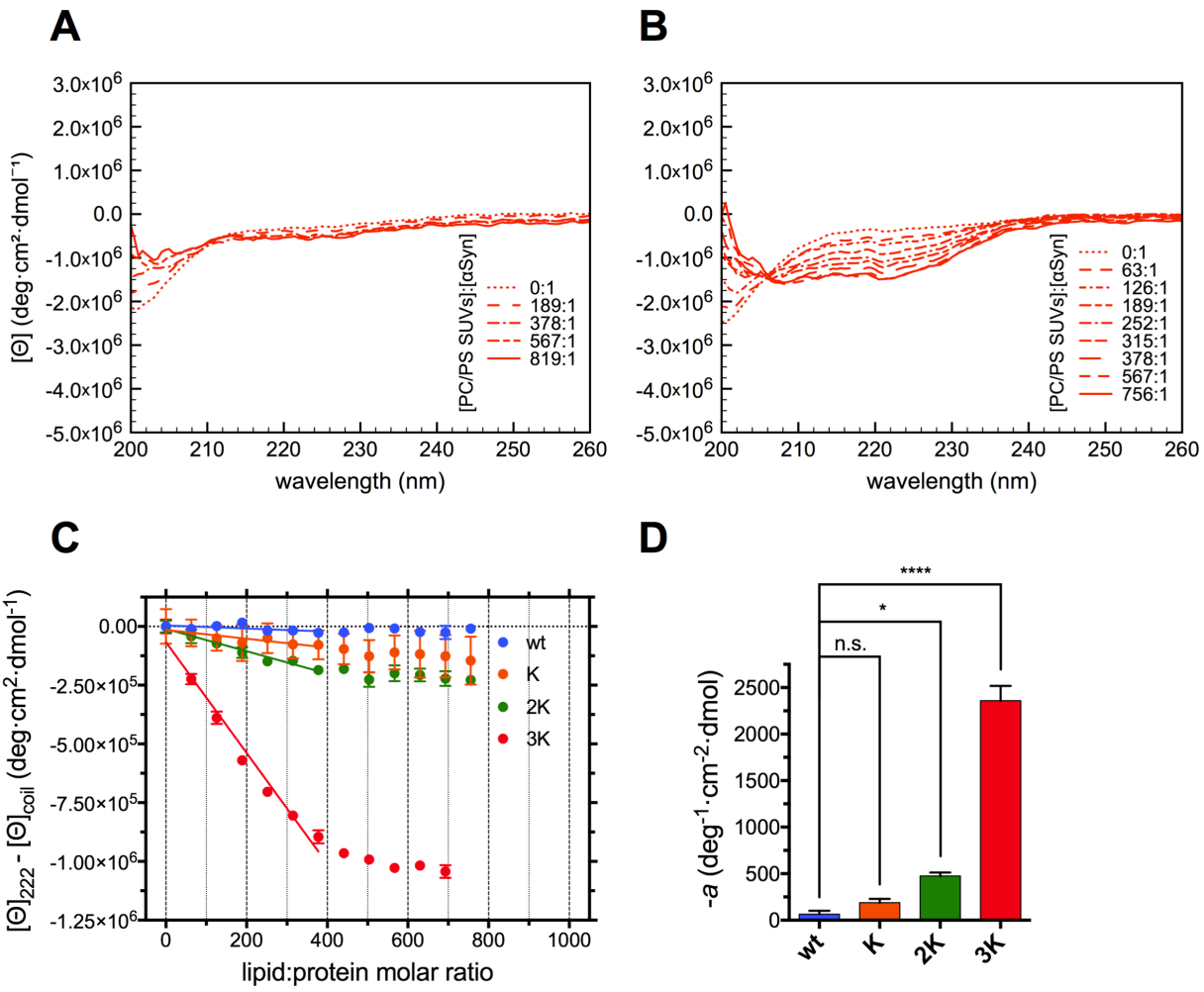

FIGURE S4. Representative far-UV CD spectra from a titration of 9.7 µM wt (*A*) and 3K (*B*) αSyn (in 9.7 mM NH_4Ac, 150 mM NaCl, pH 7.40) with 9.7 mM 70:30 POPC:DOPS LUVs, measured at 25ºC. No binding is observed in "high-salt" conditions with wt αSyn. *C*, Titration curves obtained from raw CD data after extracting the molar ellipticity at 222 nm, subtracting the unfolded ellipticity signal at the same wavelength and graphing it against the lipid:protein molar ratio at each point of the titration. Datapoints are shown along with their SEM (from n=3 independent titrations) and the best linear regression of the first 7 datapoints ($[\Theta]_{222} - [\Theta]_{coil} = a \cdot$(lipid:protein molar ratio)$+b$). *D*, Histogram of the slopes $-a$ (along with their SEM, n=3) obtained from the linear regression of the titration curves. Increasing slopes ($-a$) indicate increased binding propensity.

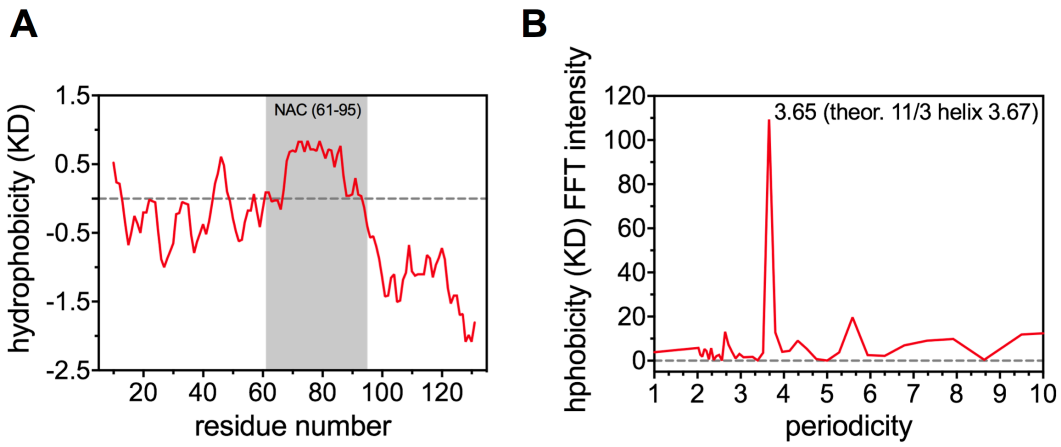

FIGURE S5. *A*, Hydropathy plot of the primary sequence of wt αSyn (1-140), calculated using the hydropathy index values of Kyte and Doolittle and averaged over a 21-residue moving window. The hydrophobicity of the primary sequence of αSyn highlights its key features: the amphipathic N-terminal region (1-95), with the slightly hydrophobic NAC domain (61-95, highlighted in gray), and the polar, negatively charged C-terminus (96-140). *B*, Fast Fourier Transform (FFT) analysis of the hydrophobicity of the N-terminus (1-95) of wt αSyn (again, the hydropathy index values of Kyte and Doolittle were used). The FFT shows a sharp maximum corresponding to the periodicity of an 11/3 helix (measured as number of residues per helix turn).

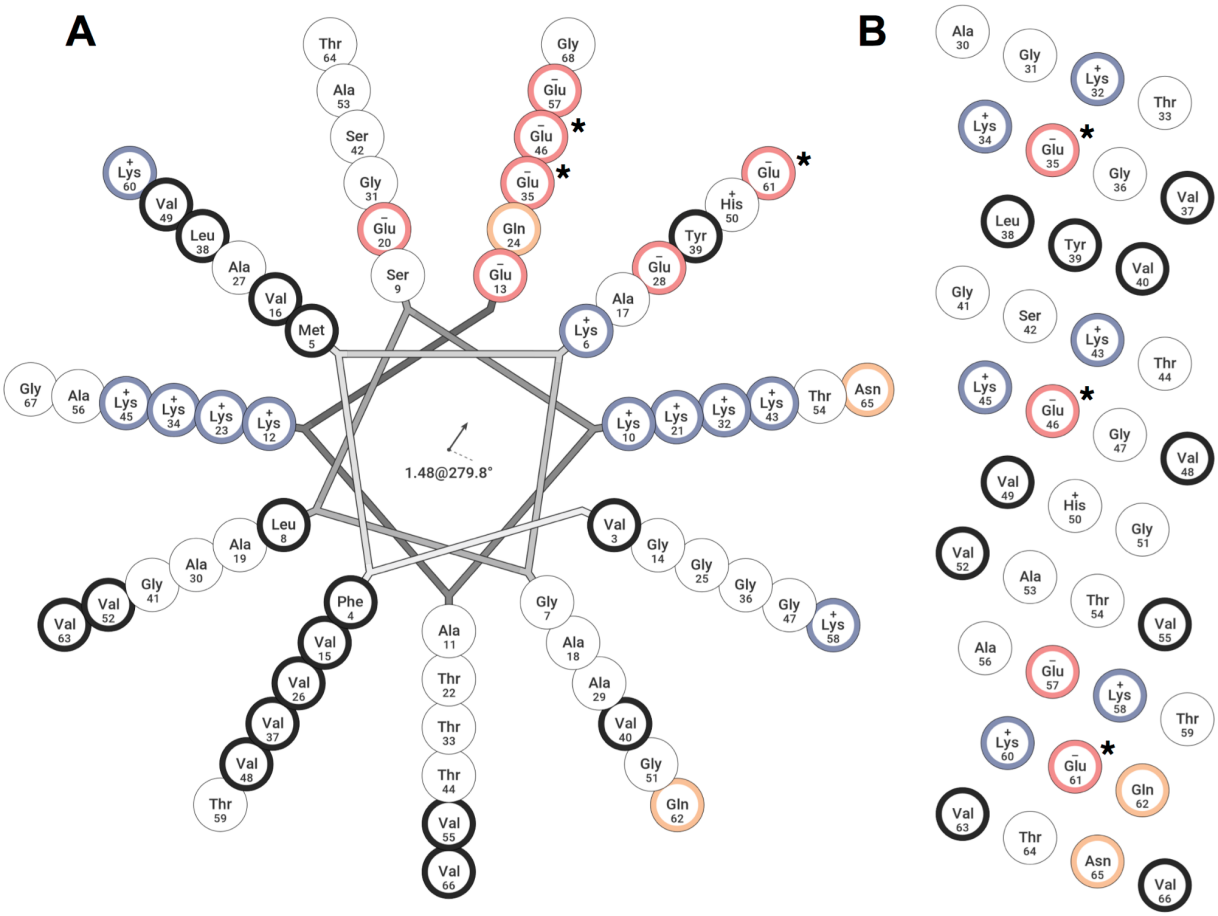

FIGURE S6. *A*, Schiffer-Edmundson helical wheel diagram of wt αSyn's N-terminal region (3-68), with the amino acids color-coded according to their polarity (Blue: positively charged aa, Red: negatively charged aa, Yellow: polar aa, White: neutral aa, Black: apolar aa). E61 is shown to be slightly closer to the membrane surface and thus comparatively better positioned to establish ionic bonds with the negatively charged lipid heads upon E-to-K mutation. *B*, Helical net diagram of the segment 30-66 of wt αSyn, color-coded as in *A*. In addition to the helical orientation, the local environment of E61 is also different from E35 and E46, suggesting that the rearrangement of electrostatic and/or hydrogen bonds upon E-to-K mutation could explain an increased 11/3 helix stability and membrane avidity.

TABLE S1 (.xlsx). ^{1}H-^{15}N HSQC spectral parameters (assigned chemical shifts and chemical shift perturbations) for Figs. 2-3.

	Hydrodynamic Radius (nm)
POPC:DOPS SUVs (sonicated)	16.4±0.9
POPC:DOPS:cholesterol SUVs (sonicated)	17.8±0.1
POPC:DOPS LUVs (extruded, 0.1 μm)	48±2

TABLE S2. DLS-measured hydrodynamic radii (along with their SEM, *n*=3) of freshly-prepared 5 mM 70:30 POPC:DOPS SUVs, 52.5:17.5:30 POPC:DOPS:cholesterol SUVs and 70:30 POPC:DOPS LUVs (extruded through a 0.1-μm polycarbonate membrane), measured at 20ºC.

CD	*N*	k_B	$-[\Theta]^{222}_{helix}$ (deg·cm²·dmol⁻¹)
wt PC:PS SUVs	157±5	$(7\pm4)\cdot10^4$	$(3.59\pm0.07)\cdot10^6$
K PC:PS SUVs	151±4 (n.s.)	$(8\pm4)\cdot10^4$ (n.s.)	$(3.83\pm0.08)\cdot10^6$ (n.s.)
2K PC:PS SUVs	148±4 (n.s.)	$(8\pm4)\cdot10^4$ (n.s.)	$(3.74\pm0.05)\cdot10^6$ (n.s.)
3K PC:PS SUVs	128±3 (**)	$(1.1\pm0.5)\cdot10^4$ (n.s.)	$(3.5\pm0.1)\cdot10^6$ (n.s.)
wt PC:PS:chol SUVs	164±3	$(8\pm2)\cdot10^4$	$(3.15\pm0.05)\cdot10^6$
K PC:PS:chol SUVs	165±3 (n.s.)	$(8\pm3)\cdot10^4$ (n.s.)	$(3.73\pm0.04)\cdot10^6$ (**)
2K PC:PS:chol SUVs	167±3 (n.s.)	$(6\pm2)\cdot10^4$ (n.s.)	$(3.44\pm0.04)\cdot10^6$ (n.s.)
3K PC:PS:chol SUVs	133±3 (***)	$(9\pm3)\cdot10^4$ (n.s.)	$(3.2\pm0.2)\cdot10^6$ (n.s.)
wt PC:PS SUVs+NaCl	90±2	$(4\pm2)\cdot10^4$	*N/A*
K PC:PS SUVs+NaCl	83±4 (n.s.)	$(5\pm4)\cdot10^4$ (n.s.)	*N/A*
2K PC:PS SUVs+NaCl	69±2 (**)	$(1.3\pm0.9)\cdot10^5$ (n.s.)	*N/A*
3K PC:PS SUVs+NaCl	72±2 (*)	$(6\pm3)\cdot10^4$ (n.s.)	*N/A*
wt PC:PS LUVs	$(8.2\pm0.2)\cdot10^2$	$(1.0\pm0.2)\cdot10^3$	$(2.54\pm0.06)\cdot10^6$
K PC:PS LUVs	$(6.3\pm0.3)\cdot10^2$ (**)	$(1.4\pm0.5)\cdot10^3$ (n.s.)	$(2.65\pm0.09)\cdot10^6$ (n.s.)
2K PC:PS LUVs	$(3.9\pm0.3)\cdot10^2$ (****)	$(1.3\pm0.4)\cdot10^3$ (n.s.)	$(2.85\pm0.07)\cdot10^6$ (*)
3K PC:PS LUVs	$(2.6\pm0.2)\cdot10^2$ (****)	$(3\pm1)\cdot10^3$ (n.s.)	$(2.93\pm0.06)\cdot10^6$ (*)

ITC	*N*	k_B	$-\Delta H$ (cal·mol⁻¹)	ΔS (cal·mol⁻¹·K⁻¹)
wt PC:PS SUVs	163±5	$(2.5\pm0.1)\cdot10^4$	290±2	19.1±0.1
K PC:PS SUVs	163±2 (n.s.)	$(2.17\pm0.08)\cdot10^4$ (n.s.)	338±3 (*)	18.7±0.1 (n.s.)
2K PC:PS SUVs	147±1 (*)	$(2.5\pm0.2)\cdot10^4$ (n.s.)	290±2 (n.s.)	19.1±0.2 (n.s.)
3K PC:PS SUVs	133±2 (***)	$(2.7\pm0.3)\cdot10^4$ (n.s.)	$(3.7\pm0.1)\cdot10^2$ (***)	19.0±0.3 (n.s.)
3K PC:PS:chol SUVs	95±8 (N/A)	$(2.3\pm0.3)\cdot10^4$ (N/A)	$(1.7\pm0.1)\cdot10^2$ (N/A)	19.3±0.3 (N/A)

CLEARANCE KINETICS	$t_{1/2}^{slow\ (abs)}$ (s^{-1})	$t_{1/2}^{fast\ (abs)}$ (s^{-1})	$t_{1/2}^{slow\ (CD)}$ (s^{-1})	$t_{1/2}^{fast\ (CD)}$ (s^{-1})
wt PC:PG MLVs	(818.3, 939.7)	(88.5, 102.2)	(926.0, 1046.0)	(125.6, 145.9)
K PC:PG MLVs	(712.3, 806.5)	(61.7, 70.6)	(615.2, 666.7)	(72.2, 84.9)
2K PC:PG MLVs	(305.3, 458.8)	(79.5, 113.3)	(300.9, 356.3)	(38.4, 64.8)
3K PC:PG MLVs	(289.4, 343.9)	(23.6, 35.6)	(419.1, 523.9)	(46.8, 67.2)

TABLE S3. Summary table of the best-fit model parameters. CD-monitored (222-nm ellipticity) titrations of wt, K, 2K, and 3K αSyn with 70:30 POPC:DOPS SUVs, 52.5:17.5:30 POPC:DOPS:cholesterol SUVs, 70:30 POPC:DOPS SUVs in 150 mM NaCl, and 70:30 POPC:DOPS LUVs; best fits obtained with an *N* independent binding sites model (*n*=3, SEMs are shown). ITC binding isotherms of wt, K, 2K, and 3K

αSyn with 70:30 POPC:DOPS SUVs and 3K αSyn with 52.5:17.5:30 POPC:DOPS:cholesterol SUVs; best fits obtained with an *N* independent binding sites model (*n*=3, SEMs are shown). Vesicle clearance kinetics of 90:10 POPC:POPG MLV dispersions by wt, K, 2K, and 3K αSyn, monitored both by absorbance at 500 nm and by CD (222-nm ellipticity); best fits obtained with a two-phase exponential decay model (95% CIs are shown). Statistical significance was determined by ordinary one-way ANOVA followed by Sidak's multiple comparisons test (vs. wt αSyn), with a single pooled variance; n.s. $p>0.05$, * $p\leq0.05$, ** $p\leq0.01$, *** $p\leq0.001$, **** $p\leq0.0001$.